Journal of Manufacturing Processes 85 (2023) 875–884

Contents lists available at ScienceDirect

Journal of Manufacturing Processes

journal homepage: www.elsevier.com/locate/manpro

Solvent triggered shape morphism of 4D printed hydrogels

Smruti Parimita [a], Amit Kumar [b], Hariharan Krishnaswamy [a,e,*], Pijush Ghosh [c,d,**]

[a] Manufacturing Engineering Section, Department of Mechanical Engineering, IIT Madras, Chennai 600036, India
[b] Department of Biotechnology, Indian Institute of Technology Madras, Chennai 600036, India
[c] Department of Applied Mechanics, Indian Institute of Technology Madras, Chennai 600036, India
[d] Center for Responsive Soft Matter, Indian Institute of Technology Madras, Chennai 600036, India
[e] Additive Manufacturing Research Group, Indian Institute of Technology Madras, Chennai 600036, India

ARTICLE INFO

Keywords:
Solvent-responsive hydrogels
Chitosan
Printability
4D printing
Soft robotics

ABSTRACT

4D printing of smart materials is a viable field of research for fabricating dynamic structures for various biomedical applications. 4D printing of hydrogel structures is challenging due to poor printability of hydrogels and poor shape fidelity of printed patterns when direct-ink writing-based 3D printers are used. In this study, chitosan (CS) hydrogel ink cross-linked with citric acid (CA) was made printable, exhibiting a shape-morphing behaviour when exposed to solvent as an external trigger. As one side of a printed structure is exposed to solvent, the solvent diffuses in and a concentration gradient is developed across the section. This concentration gradient results in displacement field, which finally leads to out-of-plane bending of the structure. This actuation is irreversible in nature since the concentration gradient is maintained between hydrophilic chitosan and hydrophobic silane layers. The reversibility of the morphed structures was achieved by dipping them in ethanol, which takes up solvent over time and thus diminishes the concentration gradient.The optimized CS/CA ink exhibited excellent rheological properties, with good extrudability and shape fidelity of printed structures. The chitosan ink was printed into various complex 3D architectures and was modified by hydrophobic coating of trimethyl silane (TMS). These hydrophobic patterns were coated on printed structures with varied interspacing, angles, and hinges to generate programmable designs. A printed soft gripper was demonstrated as an application that could lift an object seven times its weight. The shape morphing CS/CA hydrogel with excellent printability exhibits potential for 4D printing that has wide applications in soft robots, actuators, grippers, and sensors.

1. Introduction

Stimuli-responsive polymers with sophisticated functionalities have found numerous applications as soft robots and actuators [1–4], responsive medical devices, sensors [5,6], drug delivery agents [7], artificial muscles and implants [8]. Hydrogels have been widely used as "smart" materials due to their stimuli-responsive swelling and shrinking. Controllable transformation of shape can be achieved in response to various chemical and physical stimuli. Recently, solvent-responsive hydrogel thin films have been drawing attention in the field of soft robots, sensors, and actuators [9–11]. The diffusion of solvent molecules into the thin film develops a concentration gradient across its thickness which, in turn, induces a displacement field leading to out-of-plane folding. The diffusion of solvent molecules significantly influences the matrix's mechanical behaviour by altering the local arrangement of polymer chains. In turn, this changes the polymer's diffusion characteristics, establishing it as a deformation-coupled diffusion phenomenon [12].

Most of the current forming techniques to fabricate hydrogel with stimuli-responsive shape morphing are moulding [13], photolithography [14], ion dip-dyeing [15], magnetic field induction [16], patterning [17], and electrospinning [18]. These techniques are primarily limited to simple 2D film structures and impose huge limitations while fabricating complex 3D structures. Design and fabrication of a suitable mould to meet the functional requirements of a geometrically complex structure is very challenging. The incomplete polymerization and curing of the hydrogel, often encountered at the edges of such moulds, result in improper actuation. Ion-dip dyeing on the other hand, is not suitable for forming film structures beyond a certain thickness. Photolithography is limited to only photo-sensitive polymers and has difficulty developing a gradient crosslinking in a complex 3D shape. Magnetic field induction has been widely used in drug delivery applications, but the induction of magnetic field applies only to specific hydrogels with reinforced magnetic particles.

* Correspondence to: Department of Mechanical Engineering, Indian Institute of Technology Madras, Chennai 600036, India.
** Corresponding author at: Department of Applied Mechanics, Indian Institute of Technology Madras, Chennai 600036, India.
E-mail addresses: hariharan@iitm.ac.in (H. Krishnaswamy), pijush@iitm.ac.in (P. Ghosh).

https://doi.org/10.1016/j.jmapro.2022.11.065
Received 19 September 2022; Received in revised form 13 November 2022; Accepted 24 November 2022
Available online 17 December 2022

4D printing can overcome the limitations to fabricate hydrogels with enhanced flexibility of shape-morphing characteristics along with complex and rapid deformation requirements. 3D printing techniques namely, direct-ink writing(DIW), stereolithography(SLA), digital light processing(DLP), and two-photon polymerization(TPP) are in development stage for potential application of the 4D printing process of hydrogels [2,19]. SLA, DLP, and TPP can produce structures limited only to photo-polymer hydrogel inks with a single material system. DIW can print multi-material shape-morphing structures with high-resolution patterning, architectural flexibility, and unique features that respond to external stimuli [20–23]. DIW 4D printing is still in its infant research stage and the printability of hydrogels of complex structures is poor [24]. Printability of hydrogels depends on the rheology and polymerization kinetics or cross-linking [25,26]. Optimizing the hydrogel's rheological characteristics ensures smooth extrudability and good shape fidelity [27,28]. Printing parameters such as speed, pressure, nozzle diameter, and dispensing height affect the resolution and quality of the printed structure [29–32]. Hydrogels being 3D hydrophilic polymer networks, can absorb a lot of water, yet an appropriate cross linker can prevent its dissolution in water. Delay in polymerization rate may result in dimensionally unstable printed form. Rapid polymerization kinetics can clog extrusion nozzles, resulting in less precise ink deposition [33].

The choice and concentration of cross linker is an important factor in material selection.Cross linkers such as glutaraldehyde and citric acid have been used in hydrogels to impart mechanical strength, improve viscoelastic properties and reduce hydrophilicity [34,35]. Citric acid, being non-toxic, has been used as a cross linker for hydrogels. Therefore, we have used citric acid as a post cross linker in this work to improve the strength and to reduce hydrophilicity. Structures with a single polymer find limited applications, such as underwater actuation and response to multiple stimuli [16]. Bi-layer polymer structures can offer diverse solutions for several applications. These bi-polymer structures consist of a responsive and a non-responsive layer subjected to a trigger. In a recent study, chitosan-PMMA bilayer films were fabricated using solvent casting to be used as a soft gripper [12].

4D printing of solvent responsive chitosan hydrogels is rarely reported due to poor printability of chitosan using direct-ink writing technique. Seo et al. printed photo-crosslinkable temperature-reversible chitosan polymer using stereolithography process by addition of dual cross linkable hydroxybutyl methacrylated for thermal responsiveness [36]. Wu et al. 3D printed scaffolds using chitosan ink using acidic mixture of acetic, lactic and citric acid. The alkali treatment of printed structures to increase mechanical strength resulted in shrinkage of the structures, which might lead to shape-distortion of the actual printed structures [37,38]. Several works have been carried for 3D printing of chitosan with pectin, gelatin, collagen etc. but the solvent responsiveness of these structures have not been reported [39–41]. Our newly developed chitosan hydrogel has the ability to 3D print intricate shapes and even morph into complicated structures with response to solvent. The strength of the printed structures was increased by post crosslinking with citric acid without distortion of the 3D printed structures. Citric acid as a cross linker has been used to increase in strength of the chitosan films by establishing a crosslinking network between the chitosan molecules. Although this acid has been previously used as a natural cross linker of biopolymer to prepare films by solution casting and compression moulding [38,42], it has not been used as a cross linker with chitosan to prepare 3D printed structures, as carried out in this work.

In this work, we focused on developing a highly printable chitosan-based hydrogel cross-linked via citric acid with shape morphing ability for 4D printing. The printable chitosan ink was 4D printed into intricate 3D architectures and modified using trimethyl silane spray (TMS). Hydrophobic patterns were coated on printed structures with variable spacing, angles, and hinges to create programmable designs. Solvent diffusion across the thickness created a concentration gradient in these multi-material structures, facilitating actuation. This actuation is irreversible, since the concentration gradient between the chitosan and silane layer persists. The actuation can be reversed by dipping the morphed structures in ethanol, which reduces the concentration gradient by gradually absorbing the solvent. Overall, the feasibility of chitosan-based hydrogel as a novel smart material for 4D printing is examined in terms of its printability with shape-morphing capabilities.

2. Materials and methods

The chemicals such as chitosan powder (degree of deacetylation < 90%, viscosity (100–200) cps, medium molecular weight), acetic acid (extrapure AR > 99.9%), citric acid monohydrate(extrapure AR 99.7%) were supplied by SRL Chemicals Pvt. Ltd (India) and D, L-lactic acid(88%) were supplied by Merck Life Science Pvt. Ltd.(India) for the preparation of chitosan ink.

Chitosan ink was prepared by dissolving 8% (w/v) of chitosan powder in an acidic mixture (40% v/v acetic acid, 20% v/v lactic acid, 40% v/v distilled water). Around 3 wt% (out of the total weight of the acidic mixture) of citric acid was added to the solution and was kept at rest for 12 h. The solution was then mechanically stirred at 200 RPM for 2 h to dissolve the chitosan particles homogeneously, and centrifuged at 3000 RPM for 1 hour to remove air bubbles. The acidic mixture of acetic acid, lactic acid and citric acid increases the solubility of chitosan, adds mechanical strength and flexibility to the structure and minimizes drying-induced shrinkage for fabrication of different structures [37,43–47].

2.1. Rheological characterization

The chitosan-ink hydrogel was characterized using a rotational rheometer (MCR301, Anton Paar, Austria) using a 25 mm parallel plate with measurement gap of 0.55 mm. The shear thinning property, amplitude sweep and thixotropic characterization were performed at room temperature (the working temperature of the 3D printer). To study the shear-thinning property, the viscosity of the tested hydrogel ink was measured at shear rates ranging from 0.1 to 1000 s^{-1}. Strain sweeps from 0.1% to 1000% at a frequency of 1 Hz were performed to determine the linear viscoelastic region (LVR). A constant strain with LVR of 1% was chosen for the angular frequency sweeps at a range of 1–100 rad/s. The recoverability of the chitosan-ink hydrogel is correlated to the thixotropic behaviour, and the test was performed in three steps. During the first step, a shear rate of 0.1 s^{-1} was applied to the hydrogels for 60 s. This corresponds to the hydrogels preparatory stage prior to printing. The second step involves instantaneous application of high shear rate, 500 s^{-1} that was held for 10 s. This signifies the state of hydrogel under shear force during printing. In the final step, the shear rate was reduced to its initial 0.1 s^{-1} and retained for 120 s to observe the recovery of viscosity that correlates with the material behaviour post printing. The rheological measurements were carried out in order to fully characterize the gels and to relate their properties with the DIW 3D printing process.

2.2. 3D printing procedure

A custom-built 3D printer (as shown in Fig. 1) was fabricated in the lab to print chitosan ink. This customized syringe extrusion-based 3D printer works on the principle of a direct-ink writing mechanism where a highly viscous gel is extruded from the syringe. The printer is based on a core-XY 3D printer in which an extrusion nozzle can move in the X and Z axis. A separate building plate traverse along Y-axis while printing layer-by-layer to generate a 3D structure. In Fig. 1, the syringe-based extruder used compressed air pressure to feed material in a 50 mL syringe using a fluid dispensing controller (supplied by Flovell Dispensers and Systems, Maharashtra, India). The syringe extrusion 3D printer was controlled by a computer through a user interface on the printer.

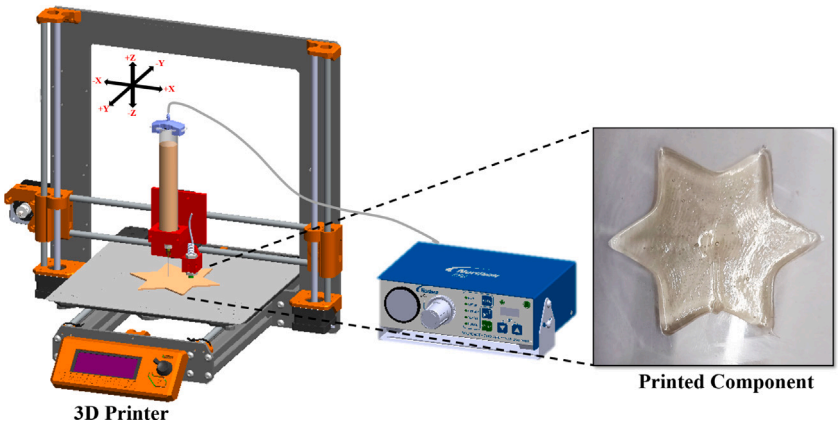

Fig. 1. Schematic representation of direct-ink writing (DIW) 3D printer with pneumatic feeding system where the printer head moves in x-axis and z-axis and the printer bed moves along y-axis.

The CAD models for 3D printing were designed using 'SolidWorks™' and were converted to '.stl' format for further pre-processing. The '.stl' files were imported into an open-source slicing software, 'Ultimaker Cura', and sliced into multiple layers based on the input parameters namely layer thickness, printing speed, infill density, and infill pattern. The prepared chitosan ink was loaded in a 50 ml syringe and mounted with the dispensing adaptor on the printer head. The printing process was carried out using a nozzle of 500 μm subjected to 5 bar pressure at a printing speed of 5 mm/s. The chitosan structures were printed onto acrylic sheets for easy detachment after drying. The printed structures were dried under vacuum at 50 °C for 24 – 48 h and cured at 150 °C for 10 min to cross-link the samples. The effect of citric acid as a cross linker in chitosan has been explained in detail in the supplementary data.

2.3. Actuation experiments of 4D printed structure

The structures were 3D printed into a multi-layered configuration, where the layers were prepared using chitosan ink (hydrophilic material) with no strip interspacing. The upper side of the printed structure was patterned by hydrophobic coating of trimethyl silane (TMS) at a specified strip interspacing and angle and the bottom side was uniformly coated. The four-layered printed structure fused during drying while the hydrophobic silane coating remained at the top and bottom surfaces of the printed structure. The actuation of all the 3D printed structures were investigated by dipping the specimens in water and ethanol. The actuation videos were recorded in real time of the experiments using a 64megapixel camera with a resolution of 1440 * 1440 and at a rate of 30fps.

To study the kinetics of the actuated structures, each of the printed structures were placed on to a glass slide. Water was injected using a micropipette in a way that the complete bottom surface of the film was in contact with the water. In case of hydrophobic coated bi-layer structures, the uncoated side was kept on the glass slide to expose it to the solvent. The folding behaviour of these printed structures were captured using an optical microscope placed perpendicular to the printed structure. A goniometer set-up was used to record the folding behaviour of as-printed and hydrophobic coated bi-layer structures. All the handling and storing of the printed structures outside the vacuum oven were performed in an air-conditioned room at 25 °C to eliminate the effects of temperature and humidity. The actuation videos were recorded using goniometer and were analysed using image processing toolbox of 'MATLAB™'. The different stages of folding of as-printed and hydrophobic coated bi-layer structures were plotted. From the plots, the total folding time, curvature of actuation and degree of folding were calculated.

The hydrogel ink was 3D printed into various designs that could transform from 3D morphologies into simple and complex 4D morphologies (such as bending, rolling, and twisting) by responding to solvent molecules.

3. Results and discussion

The results illustrate a detailed study on the solvent-responsive mechanism of the printed structures. The kinetics of the folding phenomenon was studied and explained using the diffusion characteristics of the solvent. The hydrophobic coating modified structures take more time for actuation compared to as-printed structures due to the difference in concentration gradient. An increase in bending stiffness due to additional coating material also contributes to the cause. This difference in actuation characteristics provides insight to design complicated structures with combination of pure chitosan and hydrophobic coating modified chitosan. In order to print chitosan structures, its printability was studied using the rheology characteristics of the chitosan hydrogels along with the analysis of the effect of printing parameters.

3.1. Solvent-responsive mechanism and kinetics of 4D printed structures

The 3D-printed structure (as shown in Fig. 2a) undergoes out-of-plane folding when exposed to solvent. When one side of the structure is exposed to a solvent, the solvent molecules diffuse through the polymer matrix. The number of solvent molecules decreases as one moves away from the source towards the interior of the sample. This gives rise to a concentration gradient across the thickness of the structure, as shown in Fig. 2b. The additional solvent molecules in the immediate bottom layer are accommodated by the change in curvature and thus resulting in a displacement field. This gradient of displacement or strain field generated over the layers across the thickness induces a stress field, resulting in folding or out-of-plane bending. With time, as more solvent molecules diffuse in, the through-thickness concentration gradient reduces until it vanishes completely and the film gets saturated. This restores the structure to its initial flat state. As the solvent molecules diffuse into the polymer matrix, it alters the polymer chain conformation, thus affecting its mechanical properties significantly. The deformation of polymer chains in turn affects the diffusion characteristics of the solvent across the polymer matrix. This phenomenon of folding of structure when exposed to solvent therefore emerges out as a diffusion coupled deformation phenomenon.

The as-printed structure when immersed completely in solvent does not bend, as shown in Fig. 3a. The diffusion of solvent is uniform in all the faces of the structure which results in a net-zero concentration gradient. This further confirms that the primary governing mechanism of folding of a film is the concentration gradient that develops

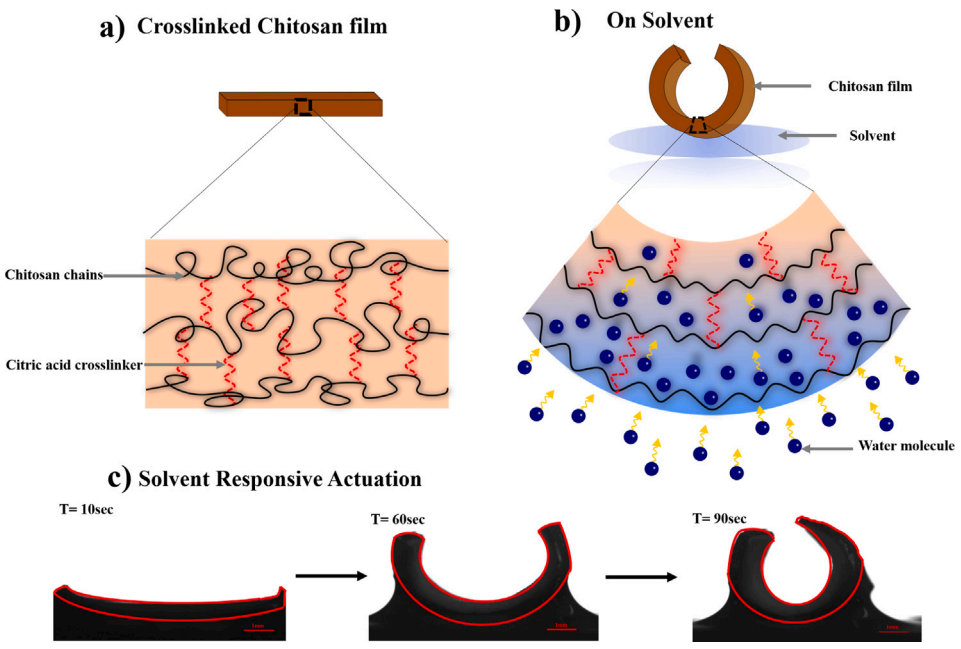

Fig. 2. Solvent responsive mechanism of actuation: (a) and (b) illustration describes the actuation of printed chitosan by the diffusion of solvent creating a concentration gradient across the thickness when kept on the surface of water, (c) snapshots of real actuation of printed chitosan (marked in red). (For interpretation of the references to colour in this figure legend, the reader is referred to the web version of this article.)

across the thickness. Applying hydrophobic coating on one face of the structure helps in building up the necessary concentration gradient for folding, as indicated in Fig. 3b. In the present work, the printed chitosan structure is modified by applying silane coating on one of its sides. Since the applied coating is hydrophobic in nature, the solvent (for example water) molecule, therefore, cannot diffuse into the coating layer. As a result, a permanent concentration gradient is formed across the thickness. The film therefore cannot saturate itself completely in spite of diffusion of solvent molecules, and thus remains permanently folded.

The kinetics of solvent responsive folding phenomenon was studied on the as-printed and hydrophobic coating modified bilayer structure using a dimension of 7 mm × 2 mm. The actuation time of the as-printed and hydrophobic modified structure was obtained and plotted (as shown in Figs. 4a and 4b). The pure chitosan structures take around 30 s for complete folding, whereas the hydrophobic coated bilayer chitosan structure takes 90 s for complete folding. The rate of change of curvature obtained is shown in Fig. 4c. The difference in time is due to the presence of a hydrophobic layer which inhibits the rate of diffusion of solvent molecules into the matrix, thus leading to slow actuation. The folded as-printed structure is reversible when solvent diffusion increases with time eliminating the concentration gradient formed across the thickness. However, permanent or irreversible folding is observed in hydrophobic modified bilayer structures, as the concentration gradient remains unaltered with time.

3.1.1. *Reversibility of printed structures applying ethanol*

The 3D printed structure can actuate and remain permanently folded, as explained above. In order to reuse the same structure, it needs to be opened or unfolded back to its initial flat condition. This can be achieved by immersing the folded structure in ethanol, as shown in Fig. 5. The ability of ethanol to unfold moisture or a vapour laden film has been reported earlier [48,49]. In this work, we have applied ethanol to unfold the permanently folded structure of chitosan. The reversibility of the folded chitosan structure to its original unfolded state is mainly due to poor solubility of chitosan in ethanol causing contraction of polymer chains and miscibility of ethanol and water. The extent of hydrogen bonding of ethanol and water is higher compared to that of chitosan molecules and water [50]. The combined effect of contraction of polymer chains and excellent miscibility of water with ethanol results in migration of water molecules from chitosan matrix to ethanol. The concentration gradient diminishes with the migration, and the printed structure returns to its original shape.

3.2. *Shape-morphing behaviour and application of 4D printed structures*

A printed structure with shape morphing abilities has broad applications in the biomedical field like sensors, actuators, and artificial valves, which require different complex structures and folding patterns. A few examples of various permanently acquired shapes of chitosan printed structures upon exposure to the solvent are demonstrated in Fig. 6. Each of these permanent folding shapes has a reversible counterpart when dipped in the ethanol solvent.

In an attempt to mimic a finger-like actuation, a rectangular strip (30 mm) was modified with hinges of 5 mm separated by a distance of 5 mm, as shown in Fig. 6a. The hydrophobic coating remained passive and did not actuate. Spiral or Helical type actuation was achieved by applying hinges of 5 mm (at 5 mm interval) at an angle of 45°as shown in Fig. 6b.

The effectiveness of hinges on actuation was explored on flower-shaped printed structures by varying the number of hinges. A structure without hinges showed greater curvature in the actuation of flaps, as there was no restriction in solvent diffusion throughout. The sample with one and two hinges actuated the flaps with prominent edge bent at the modified places. A square shaped structure was printed with edge (dimension of 30 mm) and inner flaps (with a gap of 8 mm) to mimic an artificial heart valve. The flaps of the valve opened when exposed to solvent, as shown in Fig. 6f.

As a potential soft robotic application, a gripping experiment was performed on a modified multi-finger like structure. This printed structure was able to lift an object seven times its own weight. The gripping actuation clearly demonstrates an advantage of 3D printing a structure which is mechanically robust and yet can obtain different patterned shapes useful for various biomimetic and soft robotic actuation. Figs. 7a and 7b shows the gripping and ungripping of an object respectively, demonstrating an application of a 4D printed structure as soft gripper.

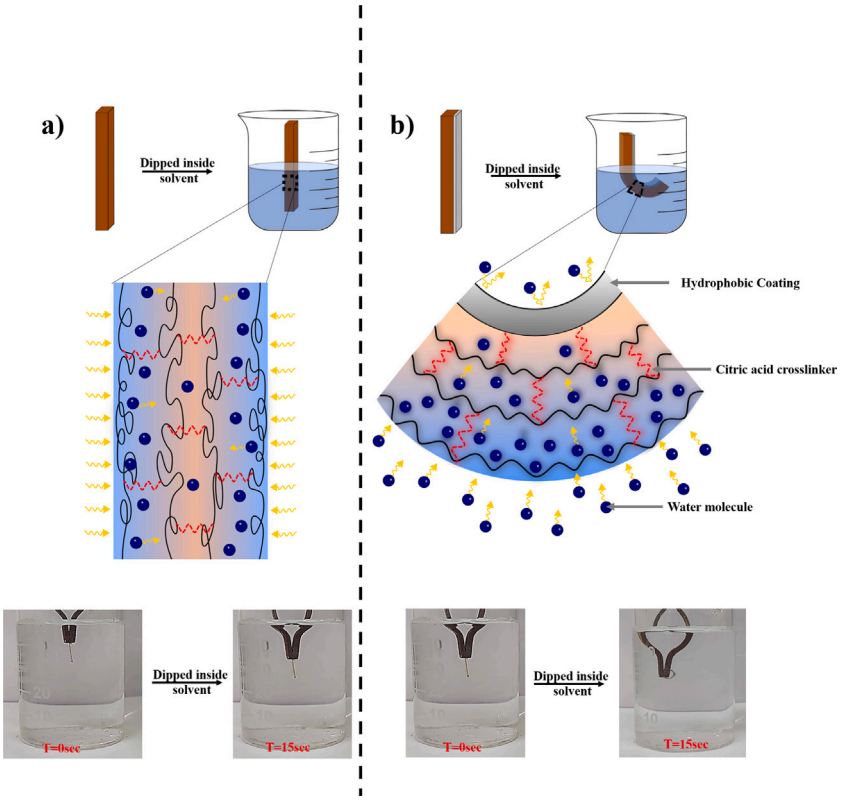

Fig. 3. Underwater actuation mechanism of silane-modified chitosan: (a) Unmodified printed chitosan when dipped inside water, solvent diffuses from both the side and concentration gradient across the thickness required for actuation is not achieved, (b) Silane modified printed chitosan being hydrophobic inhibits the diffusion from one side. A concentration gradient is generated across the thickness due to solvent diffusion from a single side leading to actuation.

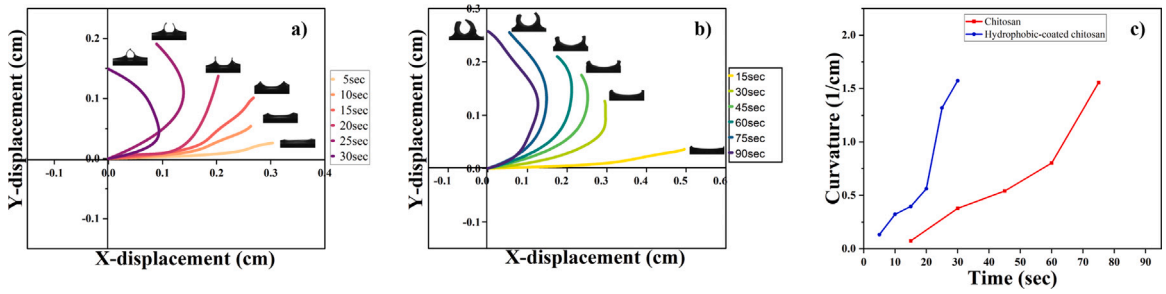

Fig. 4. Actuation of 3D printed chitosan hydrogel structures: Mechanism and kinetics (a) and (b) plot shows X–Y displacement of pure chitosan and hydrophobic modified bilayer chitosan structure respectively indicating the change in curvature when exposed to water, (c) plot indicates the curvature of chitosan and hydrophobic modified chitosan with time.

3.3. Rheological characterization for study of printability

Printability is a combined measure of both extrudability and shape fidelity. Both these behaviours are time-dependent and can be quantified by a systematic study of the rheology of hydrogels. The DIW process can be divided into three steps (as shown in Fig. 8a). Step A involves the flow of ink through the syringe, step B ejects ink from the nozzle, and step C deposits the ink onto the under-laying printed layers [51].

In order to print structures, the properties of hydrogel ink need to be carefully tailored for smooth flow through the nozzle without clogging during extrusion. From a rheology perspective, reduction of hydrogel viscosity can favour smooth extrusion through the capillary nozzle. Viscosity of hydrogel depends on temperature, pressure, velocity, and time. Since the 3D printing was carried out at isothermal conditions (at room temperature in this case). The temperature effect was not considered to vary the viscosity. It was observed that with an increase in input pressure, the viscosity of ink decreased, facilitating easy extrudability of the ink. The variation of viscosity with shear rate was studied from the shear thinning plot, which can be determined by the flow sweep test. Fig. 8b shows the outcome of a flow sweep test for an 8% chitosan hydrogel ink. Our experimentally obtained shear rate vs. viscosity plot is fit with the Ostwald–de Waele or the power law model (Eq. (1)):

$$\eta = K\dot{\gamma}^{n-1}, \tag{1}$$

where η is the viscosity of the ink, K is the flow consistency index, $\dot{\gamma}$ is the shear rate, and n is the flow behaviour or the power law index. The experimental data finds in good agreement with the power-law curve fit with R-squared=0.9988. We find that $n \approx 0.2375$, and $K \approx 1088$. $n < 1$ indicates a strong shear-thinning behaviour, in agreement with the previous studies on hydrogel inks [24,52,53]. This phenomenon results from the polymer disentanglement and macromolecular orientation along the shear flow during extrusion, which facilitates material flow.

Upon ejection of ink from the nozzle, it must rapidly stiffen to retain its shape after deposition. Viscoelastic properties of the ink employed in the DIW 3D printing process was characterized by amplitude sweep

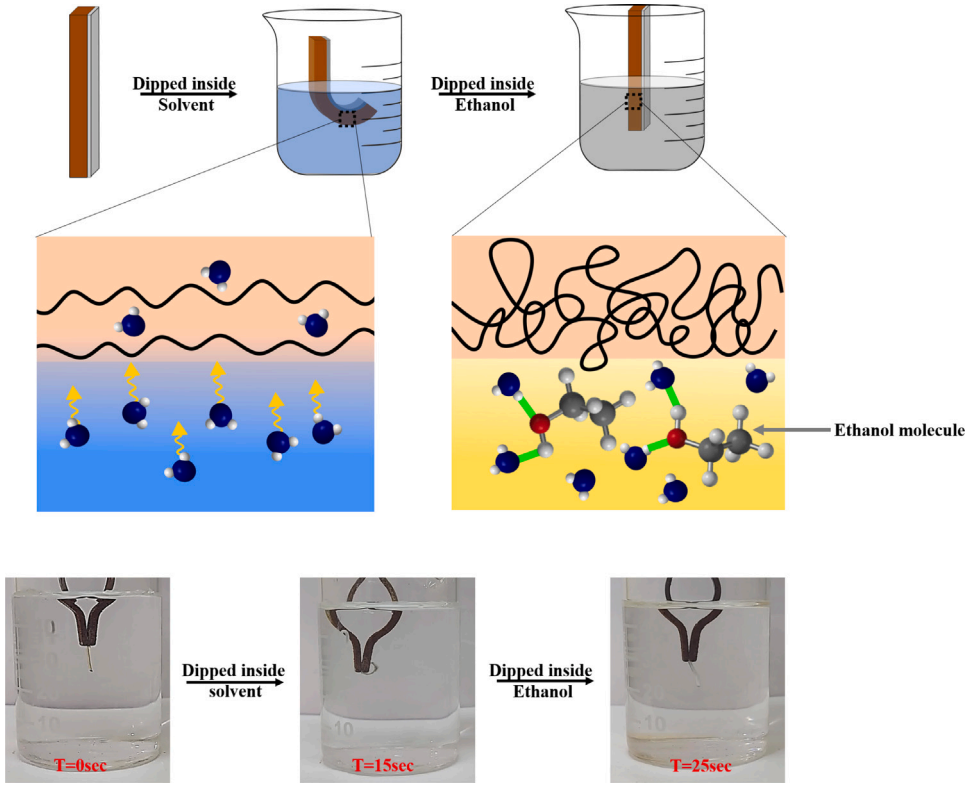

Fig. 5. Hydrophobic modified printed chitosan structure permanently folds when dipped in solvent and undergoes reversible actuation when dipped inside ethanol.

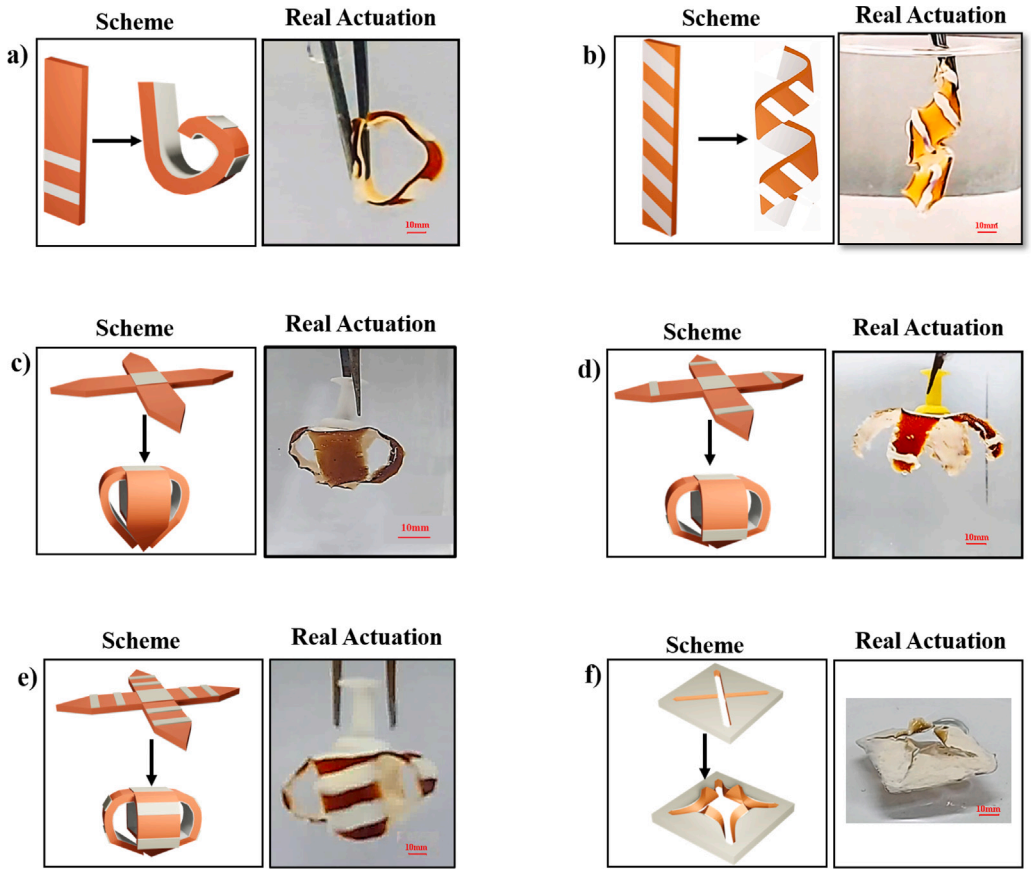

Fig. 6. 4D printed chitosan structure coated with silane acts as a hinge for different patterns of actuation: (a) finger actuation with two hinges, (b) spiral folding with diagonal hinges, (c) X-shaped printed structure without hinges actuate with curved flaps mimicking a flower, (d) X-shaped printed structure with a hinge actuate with bent flaps at the edges, (e) printed structure mimicking a gripper, and (f) Opening of valve structure.

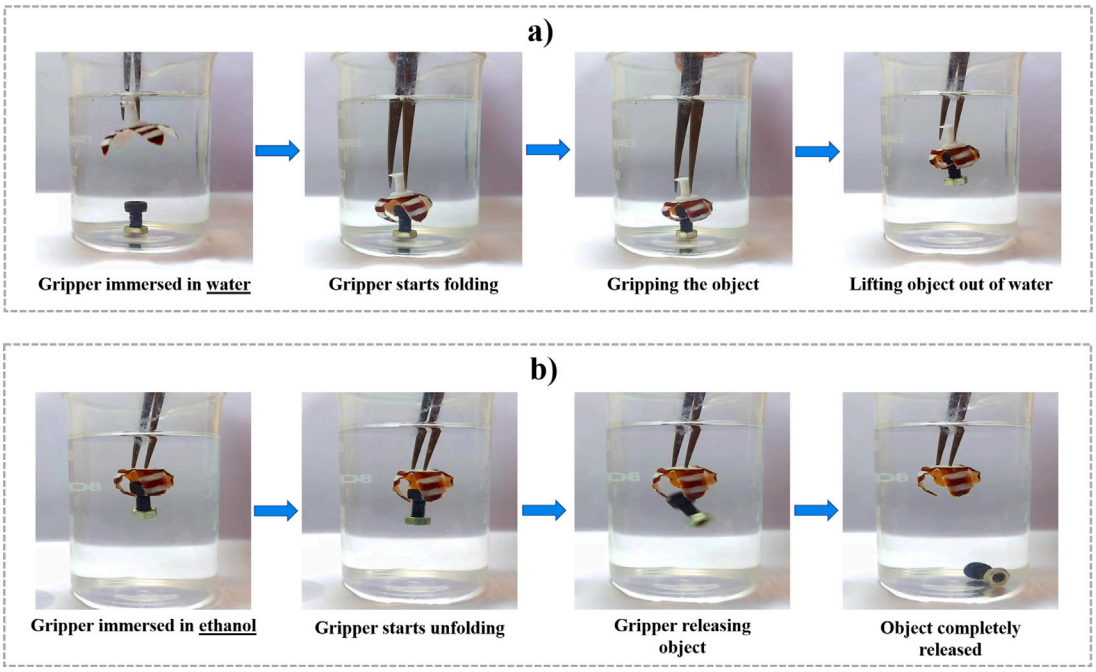

Fig. 7. Snapshots of a soft gripper: (a) gripper lifting a submerged object, (b) gripper releasing the lifted object.

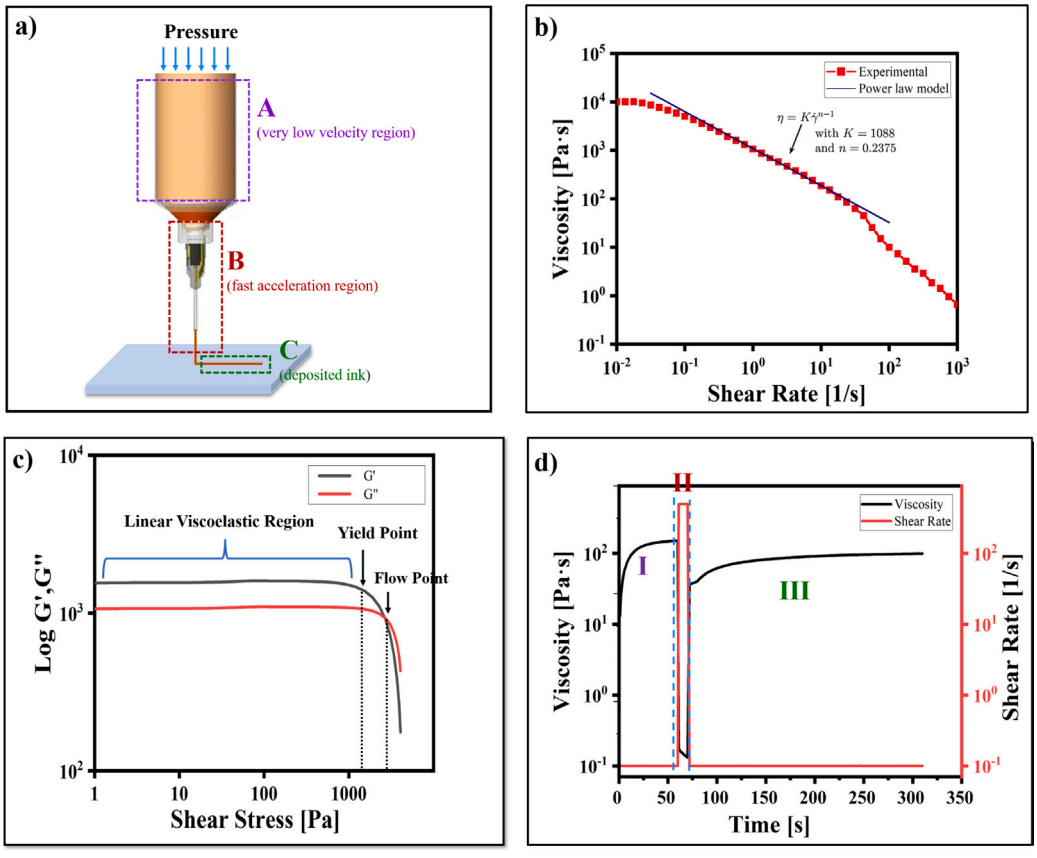

Fig. 8. Plot showing rheological characterization of chitosan ink at room temperature: (a) Rheological properties affecting printability and shape fidelity of chitosan ink (b) shear viscosity as a function of shear rate, (c) storage modulus (G') and loss modulus (G") as a function of shear stress, (d) thixotropic property.

tests (Fig. 8c). A sweep of increasing shear amplitudes was applied at a constant frequency of 1 Hz, which implies an increasing shear rate, and the evolution of loss and storage modulus [52] was measured. The first zone in Fig. 8c illustrates the linear viscoelastic region (LVR) in which the storage modulus (G') remains constant and is larger than the loss modulus (G''). $G' > G''$ correlates with higher stiffness required for retaining the shape. At a certain point, the G' value declined, the yield point and the corresponding shear stress indicated the beginning of the

breakdown of the solid structure, leading to irreversible deformation. The second region is between the yield point and flow point, where the elastic behaviour still dominates over the viscous behaviour (i.e., $G' > G''$). However, the yield stress has been overcome with an irreversible deformation. The third zone depicted the flow point where the values of G' and G'' were equal, representing the transition from rigid to viscous behaviour. Beyond the flow point, the viscous behaviour dominates over the elastic behaviour (i.e., $G' < G''$) due to progressive breakage and disentanglement of molecular structure.

To achieve a good shape fidelity during DIW, the deposited ink should exhibit a faster recovery rate. This necessitates restoration of the elastic behaviour of the material and avoids continuous flow (spreading) of the ink immediately after being deposited on the bed. This property was quantified by simulating the three-interval thixotropy test, which mimics extrusion-based printing, as illustrated in Fig. 8d. The hydrogel subjected to a shear rate of 0.1 s^{-1} was instantly increased and held for 10 s before returning to its initial 0.1 s^{-1}. The shear rate of the instantaneous loading was calculated using Eq. (2).

$$\dot{\gamma} = \frac{3n+1}{4n} \times \frac{4Q}{\pi R^3} \tag{2}$$

where n is shear thinning index obtained from flow sweep test, R is the radius of the nozzle, and Q is the volumetric flow rate of extruded hydrogel (which is calculated by measuring the volume of extruded ink when constant pressure is applied in a particular extrusion time from the nozzle of radius R) [54]. Since the nozzle wall experienced more shear stress, the maximum shear rate was estimated by considering R_{max}=R, and was 500 s^{-1} from Eq. (2). It was observed that the viscosity decreased sharply under a high shear rate of 500 s^{-1} indicating that the ink is ideally extrudable into continuous filament for printing (phase B in Fig. 8a). This phenomenon could be attributed to the breaking of physical cross-links between polymer chains by high shear stress. The shear rate was brought back to 0.1 s^{-1} and retained for 120 s to observe the viscosity recovery of the hydrogels after printing. This step simulates the rest state of the ink after being deposited on the bed (phase C in Fig. 8a). It was found that there was recovery of viscosity comparable to their initial value, indicating that the prepared chitosan ink retains its shape after printing. The recovery could be attributed to the ability of hydrogels to rebuild the broken cross-links after rest, resulting in increased and recovered viscosity.

3.4. Analysis of extrudability and shape-retention by studying printing parameters

The flowability and extrudability of the chitosan-ink were determined by extruding the ink with nozzle dia 0.5 mm by varying the printing pressure. The images taken during the extrusion process at different pressures were analysed to measure the filament diameter (d_F) and die swelling effect after extrusion. The die swelling effect was calculated from the die swelling ratio (=d_F/D) where, D is the inner diameter of the nozzle, and d_F is the diameter of the extruded filament. Fig. 9a shows the effect of the extrusion pressure on die swelling and filament size when a 8 wt% chitosan solution was extruded. The filament diameter and die swelling ratios increase with extrusion pressure because the chitosan molecules are aligned under higher pressure and tend to relax when extruded out of the nozzle in a low-stress environment.

3D printing of structures requires good rheological properties and precise control of the applied pressure at an appropriate printing speed using a micronozzle. The extrusion pressure is an essential printing parameter, which helps to determine the extrusion output, as it directly affects the printed line width. The application of low extrusion pressure would be insufficient to squeeze the ink out of the nozzle. On the other hand, high extrusion pressure leads to instability of extruded ink which is hard to control, resulting in poor printability. The optimal condition of the parameter was selected as the one allowing for the continuous extrusion of structurally stable 3D structures. In particular, 1 – 7 bar pressure values were considered. Pressure=1 bar was not sufficient to extrude the hydrogel through the needle. Pressure=2–6 bar allowed for the extrusion of a continuous and steady fibre. Pressure=7 bar resulted in dispersion of the cluster of material as shown in fig.S4. Since a continuous and steady fibre was obtained using an extrusion pressure ranging from 2 – 6 bar, therefore a suitable range of pressure(2 – 6 bar) can be chosen for the nozzle with dia 0.5 mm to obtain good quality print. We selected 5 bar pressure to study the effect of printing speed on the layer thickness and line width. In particular, 1–10 mm/s printing speed were considered. A single fibre diameter was reported as the printing speed varies, which was quantified using layer thickness and line width, as shown in Fig. 9b. The line width and layer thickness images were taken during printing using a digital microscope (Model no: VIBOTON Wi-Fi digital microscope) and analysed using 'ImageJ'. With increasing in the speed values, the 3D printer does not have enough time to deposit the ink, resulting in progressive fibre thinning or lack of deposition of ink on the surface of the build platform. Slower speed(i.e. 1, 2, 3, 4 mm/s) resulted in larger variation of line width in comparison to nozzle diameter of 0.5 mm. Higher speed(i.e. 8 – 10 mm/s), a shear thinning of the fibres and lack of deposited hydrogel were observed at some points in Fig. 9b and S5 resulting in discontinuous printed structures. This study provides insights into corresponding input parameters such as printing speed, printing pressure, nozzle diameter, and layer thickness during the slicing of the 3D model. Based on the study, a set of printing parameters (nozzle diameter 0.5 mm, printing pressure 5 bar, and printing speed 5mm/s) was chosen to print complex structures. The quantified error in layer thickness and line width (obtained using image analysis) were added and given as input parameters in the slicing software.

Various shapes were printed using the optimized printing parameters as shown in Fig.S6 and compared with the CAD model to study the shape fidelity of the printed structures. The results in the image showed that the printed structures were as per the dimensions of the designed part. These results confirm that the optimized ink had a good printability and shape fidelity using the custom designed 3D printer.

In this work, a novel chitosan-hydrogel ink for 4D printing is demonstrated. The rheological characterization is an important parameter to study the printability of ink. The 3D printed structures can be actuated and reversed by appropriate surface treatment using different solvents. The printing parameters for 3D printing of the objects are sensitive to both the material properties and complexity in geometry. Work on complex designs with different shape morphing features is under progress in evaluation.

4. Conclusions

In this work, a simple method for 4D printing of chitosan as hydrogel cross-linked with citric acid exhibiting desirable shape morphing behaviour is proposed. The printability of chitosan ink was determined by studying the rheological properties and optimizing printing parameters such as printing speed, printing pressure, and nozzle diameter. The printed structures were modified applying spray coating with hydrophobic silane for actuation under solvent. We observed that the modified structures resulted in permanent (irreversible) folding. The reversibility of the permanently folded structure was achieved by immersing the structures in ethanol. Hydrophobic patterns were created to program a shape-morphing behaviour, resulting in complex 3D morphologies, thus miming a finger, a creeper, and a flower upon immersion in water. As an application in soft robotics, we demonstrated a soft gripper actuator by lifting an object from solvent (water) and releasing it by unfolding it in ethanol. Due to its excellent printability, biocompatibility, and shape-morphing ability, our newly developed chitosan hydrogel ink demonstrates significant potential for fabricating a diverse range of dynamic architectures finding applications in the biomedical field, food industry, and electronics industry.

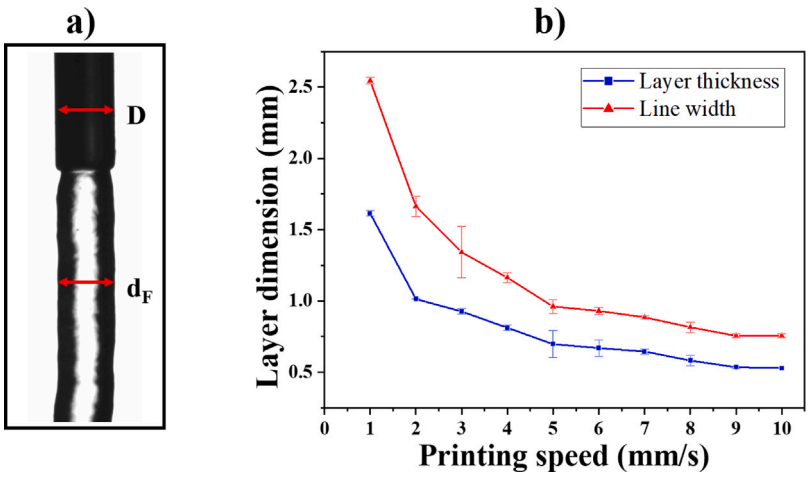

Fig. 9. Study of printing parameters: (a) die swelling effect, (b) variation of layer thickness and line width with printing speed.

Declaration of competing interest

The authors declare that they have no known competing financial interests or personal relationships that could have appeared to influence the work reported in this paper.

Acknowledgements

This research work was not funded by any governmental, private, or non-profit funding bodies.

Appendix A. Supplementary data

Supplementary material related to this article can be found online at https://doi.org/10.1016/j.jmapro.2022.11.065.

References

[1] Ge L, Dong L, Wang D, Ge Q, Gu G. A digital light processing 3D printer for fast and high-precision fabrication of soft pneumatic actuators. Sensors Actuators A 2018;273:285–92.
[2] Khalid MY, Arif ZU, Ahmed W, Umer R, Zolfagharian A, Bodaghi M. 4D printing: Technological developments in robotics applications. Sensors Actuators A 2022;113670.
[3] Shiblee MNI, Ahmed K, Kawakami M, Furukawa H. 4D printing of shape-memory hydrogels for soft-robotic functions. Adv Mater Technol 2019;4(8):1900071.
[4] Wang X, Xu T, Andrade MJd, Rampalli I, Cao D, Haque M, et al. The interfacial shear strength of carbon nanotube sheet modified carbon fiber composites. In: Challenges in mechanics of time dependent materials, Vol. 2. Springer; 2021, p. 25–32.
[5] Hu J, Liu S. Responsive polymers for detection and sensing applications: Current status and future developments. Macromolecules 2010;43(20):8315–30.
[6] Cao D, Malakooti S, Kulkarni VN, Ren Y, Liu Y, Nie X, et al. The effect of resin uptake on the flexural properties of compression molded sandwich composites. Wind Energy 2022;25(1):71–93.
[7] Hu X, Ge Z, Wang X, Jiao N, Tung S, Liu L. Multifunctional thermo-magnetically actuated hybrid soft millirobot based on 4D printing. Composites B 2022;228:109451.
[8] Lendlein A, Kelch S. Shape-memory polymers as stimuli-sensitive implant materials. Clin Hemorheol Microcirc 2005;32(2):105–16.
[9] Chen J-K, Chang C-J. Fabrications and applications of stimulus-responsive polymer films and patterns on surfaces: A review. Materials 2014;7(2):805–75.
[10] Mandal S, Vignesh A, Debnath S, Ojha U. Mechanically robust anisotropic hydrogel–organogel conjugates for soft actuators with fast response time and diverse bi-axial programmable folding ability. Chem Mater 2022.
[11] Cao D, Malakooti S, Kulkarni VN, Ren Y, Lu H. Nanoindentation measurement of core–skin interphase viscoelastic properties in a sandwich glass composite. Mech Time-Depend Mater 2021;25(3):353–63.
[12] Meena RK, Rapaka SD, Pratoori R, Annabattula RK, Ghosh P. An embedded interface regulates the underwater actuation of solvent-responsive soft grippers. Soft Matter 2022;18(2):372–81.
[13] Yao C, Liu Z, Yang C, Wang W, Ju X-J, Xie R, et al. Poly (N-isopropylacrylamide)-clay nanocomposite hydrogels with responsive bending property as temperature-controlled manipulators. Adv Funct Mater 2015;25(20):2980–91.
[14] Wang ZJ, Hong W, Wu ZL, Zheng Q. Site-specific pre-swelling-directed morphing structures of patterned hydrogels. Angew Chem Int Ed 2017;56(50):15974–8.
[15] Peng X, Li Y, Zhang Q, Shang C, Bai Q-W, Wang H. Tough hydrogels with programmable and complex shape deformations by ion dip-dyeing and transfer printing. Adv Funct Mater 2016;26(25):4491–500.
[16] Erb RM, Sander JS, Grisch R, Studart AR. Self-shaping composites with programmable bioinspired microstructures. Nature Commun 2013;4(1):1–8.
[17] Yoon C, Xiao R, Park J, Cha J, Nguyen TD, Gracias DH. Functional stimuli responsive hydrogel devices by self-folding. Smart Mater Struct 2014;23(9):094008.
[18] Štular D, Kruse M, Župunski V, Kreinest L, Medved J, Gries T, et al. Smart stimuli-responsive polylactic acid-hydrogel fibers produced via electrospinning. Fibers Polym 2019;20(9):1857–68.
[19] Baker AB, Bates SR, Llewellyn-Jones TM, Valori LP, Dicker MP, Trask RS. 4D printing with robust thermoplastic polyurethane hydrogel-elastomer trilayers. Mater Des 2019;163:107544.
[20] Lewis JA. Direct ink writing of 3D functional materials. Adv Funct Mater 2006;16(17):2193–204.
[21] Rafiee M, Farahani RD, Therriault D. Multi-material 3D and 4D printing: A survey. Adv Sci 2020;7(12):1902307.
[22] Saadi M, Maguire A, Pottackal NT, Thakur MSH, Ikram MM, Hart AJ, et al. Direct ink writing: A 3D printing technology for diverse materials. Adv Mater 2022;2108855.
[23] Zhu H, He Y, Wang Y, Zhao Y, Jiang C. Mechanically-guided 4D printing of magnetoresponsive soft materials across different length scale. Adv Intell Syst 2022;4(3):2100137.
[24] Lai J, Ye X, Liu J, Wang C, Li J, Wang X, et al. 4D printing of highly printable and shape morphing hydrogels composed of alginate and methylcellulose. Mater Des 2021;205:109699.
[25] Gao T, Gillispie GJ, Copus JS, Pr AK, Seol Y-J, Atala A, et al. Optimization of gelatin–alginate composite bioink printability using rheological parameters: A systematic approach. Biofabrication 2018;10(3):034106.
[26] Kim JH, Yoo JJ, Lee SJ. Three-dimensional cell-based bioprinting for soft tissue regeneration. Tissue Eng Regen Med 2016;13(6):647–62.
[27] Klar V, Pere J, Turpeinen T, Kärki P, Orelma H, Kuosmanen P. Shape fidelity and structure of 3D printed high consistency nanocellulose. Sci Rep 2019;9(1):1–10.
[28] Habib MA, Khoda B. Rheological analysis of bio-ink for 3D bio-printing processes. J Manuf Process 2022;76:708–18.
[29] Dingeldein JC, Walczak KA, Swatowski BW, Friedrich CR, Middlebrook CT, Roggemann MC. Process characterization for direct dispense fabrication of polymer optical multi-mode waveguides. J Micromech Microeng 2013;23(7):075015.
[30] He Y, Yang F, Zhao H, Gao Q, Xia B, Fu J. Research on the printability of hydrogels in 3D bioprinting. Sci Rep 2016;6(1):1–13.
[31] Rao RB, Krafcik KL, Morales AM, Lewis JA. Microfabricated deposition nozzles for direct-write assembly of three-dimensional periodic structures. Adv Mater 2005;17(3):289–93.
[32] Barletta M, Gisario A, Mehrpouya M. 4D printing of shape memory polylactic acid (PLA) components: Investigating the role of the operational parameters in fused deposition modelling (FDM). J Manuf Process 2021;61:473–80.
[33] Ning L, Chen X. A brief review of extrusion-based tissue scaffold bio-printing. Biotechnol J 2017;12(8):1600671.

[34] Khouri J, Penlidis A, Moresoli C. Viscoelastic properties of crosslinked chitosan films. Processes 2019;7(3):157.
[35] Rath A, Mathesan S, Ghosh P. Folding behavior and molecular mechanism of cross-linked biopolymer film in response to water. Soft Matter 2016;12(45):9210–22.
[36] Seo JW, Shin SR, Park YJ, Bae H. Hydrogel production platform with dynamic movement using photo-crosslinkable/temperature reversible chitosan polymer and stereolithography 4D printing technology. Tissue Eng Regen Med 2020;17(4):423–31.
[37] Wu Q, Therriault D, Heuzey M-C. Processing and properties of chitosan inks for 3D printing of hydrogel microstructures. ACS Biomater Sci Eng 2018;4(7):2643–52.
[38] Nataraj D, Sakkara S, Meghwal M, Reddy N. Crosslinked chitosan films with controllable properties for commercial applications. Int J Biol Macromol 2018;120:1256–64.
[39] Elviri L, Foresti R, Bergonzi C, Zimetti F, Marchi C, Bianchera A, et al. Highly defined 3D printed chitosan scaffolds featuring improved cell growth. Biomed Mater 2017;12(4):045009.
[40] Suo H, Zhang J, Xu M, Wang L. Low-temperature 3D printing of collagen and chitosan composite for tissue engineering. Mater Sci Eng: C 2021;123:111963.
[41] Zhou L, Ramezani H, Sun M, Xie M, Nie J, Lv S, et al. 3D printing of high-strength chitosan hydrogel scaffolds without any organic solvents. Biomater Sci 2020;8(18):5020–8.
[42] Guerrero P, Muxika A, Zarandona I, De La Caba K. Crosslinking of chitosan films processed by compression molding. Carbohydr Polymers 2019;206:820–6.
[43] Roy JC, Salaün F, Giraud S, Ferri A, Chen G, Guan J. Solubility of chitin: Solvents, solution behaviors and their related mechanisms. Solubility Polysacch. 2017;3:20–60.
[44] Bégin A, Van Calsteren M-R. Antimicrobial films produced from chitosan. Int J Biol Macromol 1999;26(1):63–7.
[45] Rinaudo M, Pavlov G, Desbrieres J. Influence of acetic acid concentration on the solubilization of chitosan. Polymer 1999;40(25):7029–32.
[46] Niamsa N, Baimark Y, et al. Preparation and characterization of highly flexible chitosan films for use as food packaging. Am J Food Technol 2009;4(4):162–9.
[47] Romanazzi G, Gabler FM, Margosan D, Mackey BE, Smilanick JL. Effect of chitosan dissolved in different acids on its ability to control postharvest gray mold of table grape. Phytopathology 2009;99(9):1028–36.
[48] Haldorai Y, Shim J-J. Chemo-responsive bilayer actuator film: Fabrication, characterization and actuator response. New J Chem 2014;38(6):2653–9.
[49] Toncheva A, Willocq B, Khelifa F, Douheret O, Lambert P, Dubois P, et al. Bilayer solvent and vapor-triggered actuators made of cross-linked polymer architectures via Diels–Alder pathways. J Mater Chem B 2017;5(28):5556–63.
[50] Ozmen MM, Okay O. Swelling behavior of strong polyelectrolyte poly (Nt-butylacrylamide-co-acrylamide) hydrogels. Eur Polym J 2003;39(5):877–86.
[51] Tagliaferri S, Panagiotopoulos A, Mattevi C. Direct ink writing of energy materials. Mater Adv 2021;2(2):540–63.
[52] del Mazo-Barbara L, Ginebra M-P. Rheological characterisation of ceramic inks for 3D direct ink writing: A review. J Eur Ceram Soc 2021;41(16):18–33.
[53] Jin H, Jia D, Yang Z, Zhou Y. Direct ink writing of Si2N2O porous ceramic strengthened by directional β-Si3N4 grains. Ceram Int 2020;46(10):15709–13.
[54] Peak CW, Stein J, Gold KA, Gaharwar AK. Nanoengineered colloidal inks for 3D bioprinting. Langmuir 2018;34(3):917–25.